A Novel Chirp Detector Algorithm for Universal Pantograph Arc Detection

Mohamed S. Elbelkasi
Electrical Engineering Department, Faculty of Engineering, Mansoura University, Mansoura, Egypt | Faculty of Engineering, Mansoura National University, Gamasa, Egypt
m_elbelkasi@mans.edu.eg (corresponding author)

Nagy I. Elkalashy
Electrical Engineering Department, Faculty of Engineering, Menoufia University, Shebin Elkom, Egypt
nagy.elkalashy@sh-eng.menofia.edu.eg

Ebrahim A. Badran
Electrical Engineering Department, Faculty of Engineering, Mansoura University, Mansoura, Egypt | Mansoura Higher Institute of Engineering and Technology, Mansoura College, Mansoura, Egypt
ebadran@mans.edu.eg

Mansour H. Abdel-Rahman
Electrical Engineering Department, Faculty of Engineering, Mansoura University, Mansoura, Egypt
rahman@mans.edu.eg

Received: 8 September 2025 | Revised: 25 September 2025 | Accepted: 10 October 2025

 DOI: https://doi.org/10.48084/etasr.14604

ABSTRACT

Catenary-pantograph arc faults pose a serious threat to the reliability and safety of electric railways. Faults cause violent transient disturbances, accelerate equipment aging, and disrupt power continuity. Real-time applicability is limited for traditional approaches based on their reliance on image processing or vision-based deep learning and their computation latency is greater than the arc time constant. The paper introduces a novel image-free arc detection algorithm that directly processes measured pantograph current signals without relying on vision data. The novelty of the chirp-inspired algorithm lies in integrating band-pass filtering, differentiation, Hilbert transform envelope extraction, and multi-stage statistical processing to construct an efficient arc detection index. In contrast to existing approaches, the algorithm exploits the inherent physical fingerprints of arc transients in the electrical current waveform, representing the first systematic investigation into current-based arc detection in pantograph–catenary systems. The approach is evaluated across 20 test cases under varying arc time constants and fixed voltages to demonstrate its universality. The algorithm consistently distinguishes arc events from mechanical or noise-induced oscillations, providing a stable baseline after arc extinction and enabling real-time and reliable monitoring. The proposed image-free system surpasses vision-based schemes for arc detection, providing a scalable and feasible solution to leading-edge railway electrification systems.

Keywords-image-free arc detection; Hilbert transform; pantograph–catenary system; series arc detection; real-time pantograph arc monitoring

I. INTRODUCTION

The pantograph–catenary interface is utilized to consistently and efficiently transfer electric energy from the overhead contact line to the train. However, this interface is prone to arc faults arising from intermittent discharges during mechanical separation, vibration, or environmental disturbances. These arcs compromise the system's reliability by wearing the contact strip and injecting disruptive transients into the traction network [1].

Image-based techniques complemented by signal processing methods have been employed to study arc detection in pantograph–catenary systems. Vision-based detection combined with deep learning can provide accurate identification of arcs [2-7]. Nevertheless, this approach has its limitations for real-time railway applications because of its heavy computational requirements. Additionally, it lacks a suitable arc model for evaluating arc behavior under different operating conditions. In parallel, signal processing methods, such as the Discrete Wavelet Transform (DWT) and Hilbert–

Huang Transform (HHT), have been applied in the context of arc image analysis, exploiting their time–frequency localization to capture transient events [3, 8-12]. These methods have not been applied in the detection of the electrical characteristics of series arcing faults, which are inherently embedded in pantograph–catenary systems. The need for approaches that directly utilize the electrical signatures of arcs rather than external image-based indicators is evident.

Robust arc models are critical in advancing arc detection using current and voltage. Existing modeling frameworks attempt to unify the description of arcs across different applications, considering geometric, electrical, environmental, and dynamic factors. In pantograph–catenary systems, the arc time constant (τ) and stationary voltage (U_{st}) are the governing parameters that determine the arc persistence, reignition, and extinction [13-16]. The accurate modeling of these parameters under varying operating conditions is essential for understanding the arc dynamics and to test detection algorithms in realistic scenarios.

Existing arc detection methods, with limited robustness, use either image-based techniques [2, 5-7] or a conventional signal processing method [3, 8-12]. Vision-based methods are accurate in controlled settings but are sensitive to changes in illumination, weather, and pantograph speed. Similarly, signal-based algorithms have demonstrated promising detection capabilities in nominal or steady-state scenarios. The combined effects of sudden operating condition changes and measurement noise are yet to be examined. The modeling efforts in [13–18] acknowledge these coupled challenges, but they primarily emphasize arc characterization rather than robust detection.

To address these limitations, a novel image-free arc detection algorithm is proposed that utilizes only measured pantograph–catenary current signals. By transforming the current derivative using the Hilbert envelope and applying a hierarchical statistical framework, the method extracts discriminative arc signatures while rejecting noise and mechanical oscillations. In contrast to conventional vision-based approaches, this technique directly exploits the electrical fingerprint of arcs. Evaluation has been conducted across a wide range of stationary voltages and arc time constants to confirm the robust performance of the proposed algorithm under both weak and strong arc conditions.

II. SCOPE OF ARC MODELING

The accurate modeling of electric arcs is essential for understanding their behavior under different operating conditions. The arc presents nonlinear characteristics attributed to several randomly occurring factors. The current density defines the energy input to the arc. As the current density increases, the arc temperature increases, thus changing its stability and shape. In addition, environmental aspects, such as gas pressure, humidity, and the surrounding medium, further influence the arc's behavior [17, 18]. Consequently, the development of reliable arc models is critical to analyze the arc dynamics and design and evaluate a wide range of electrical systems.

Arc modeling can be applied in fields including circuit breakers, transmission and distribution systems, electric arc furnaces, and pantograph–catenary systems in high-speed railways [17–19]. In [14-17], the arc is treated using black-box models, where it is simplified as an electrical component without considering the plasma processes inside the arc channel. While this simplification can be useful for system-level analysis, it fails to include the physical interactions controlling the arc dynamics.

The arc conductance model is built on the balance between the energy provided by the current density and the power dissipated to the surrounding atmosphere. This balance is usually described by a general arc equation that relates the electrical properties of the arc to the mechanisms of energy input and energy loss [14]. The basic formulation of this relationship can be written as:

$$\frac{dg}{dt} = \frac{1}{\tau}(G - g) \quad (1)$$

where g represents the dynamic arc conductance, which changes with time. The governing equation is defined by two key parameters: τ and the stationary arc conductance G. The arc parameter G in (1) can be simplified to a short arc parameter that is:

$$G = \frac{|i|}{U_{st}} \quad (2)$$

where $|i|$ is the absolute arc current and U_{st} is simply estimated from the arc voltage waveform, which is the arc voltage at the instantaneous peak current. These parameters are variables on the other factors depending on the applications and arc characteristics [13].

Arc modeling operates under different electrical and environmental conditions in each system it is applied. For instance, in circuit breakers, magnetohydrodynamic-based models combine fluid dynamics, thermodynamics, and electromagnetism. This combination explains arc extinction as a balance between the energy supplied and the thermal losses, where conductivity varies strongly with temperature [18]. On the other hand, fault arc models capture the random and recurring nature of arcing in power systems. These models rely on statistical methods to characterize voltage–current signatures while considering changes in load, conductor materials, and environmental factors [14]. Pantograph arc modeling incorporates time-varying parameters and probabilistic distributions to represent the effects of speed, mechanical vibrations, and weather on arc ignition, duration, and extinction [1]. Other pantograph–catenary models have explored fuzzy regulation methods but have not directly addressed arc detection [18]. Electric arc furnaces require models capable of representing a highly nonlinear, chaotic arc behavior and its impact on power quality, linking electrode position, arc length, and electrical parameters in real time [19, 20].

In railway applications, pantograph arc modeling mainly considers the electrical interaction between the pantograph and the overhead line. The arc is affected by factors such as train speed, mechanical vibration, and environmental conditions like humidity and temperature [1]. Given that these conditions

change in a random way, the arc shows stochastic behavior. To reflect this variability, the parameters of the arc model in (1) are defined over a broad range, which makes the model more capable of representing the actual arc behavior.

III. ARC REPRESENTATION

The arc model described by (1) depends on electrical, dynamic, environmental, and geometrical factors. The electrical factors include current density, voltage level, and frequency of operation. Dynamic factors are related to motion, acceleration, and contact force. Environmental influences like temperature, humidity, and pressure also shape the arc, together with geometrical aspects such as arc length, electrode design, and plasma channel structure [13–18]. In (1), the arc behavior is defined by τ and U_{st}, which, when taken within their practical ranges, provide a general representation of pantograph arcing.

The arc's dynamic behavior is a result of the quantity of energy going into the plasma compared to the one lost. Among the factors affecting the energy input, the electrical ones have the greatest effect. Higher current levels increase conductivity and lead to lower stationary voltage and shorter time constants. In AC pantograph–catenary systems, a higher operating frequency has a similar effect, improving conductivity and reducing the stationary voltage. On the other hand, energy dissipation is controlled by environmental and dynamic factors. For instance, a higher train speed increases the stationary voltage but shortens the time constant, while a stronger contact force lowers both values.

The stationary voltage is assumed to fluctuate between 500 and 2500 V, while τ is between 1 and 100 µs to represent the variability of the arc channels in pantograph–catenary systems [1]. Figure 1 presents the voltage–current (V–I) characteristics for different time constants at U_{st} equal to 1500 V. Figure 1 reveals that the hysteresis loop area increases as τ becomes larger, indicating enhanced energy dissipation. In addition, the arc sharpness decreases with increasing τ, reflecting a reduction in the transient responsiveness of the arc.

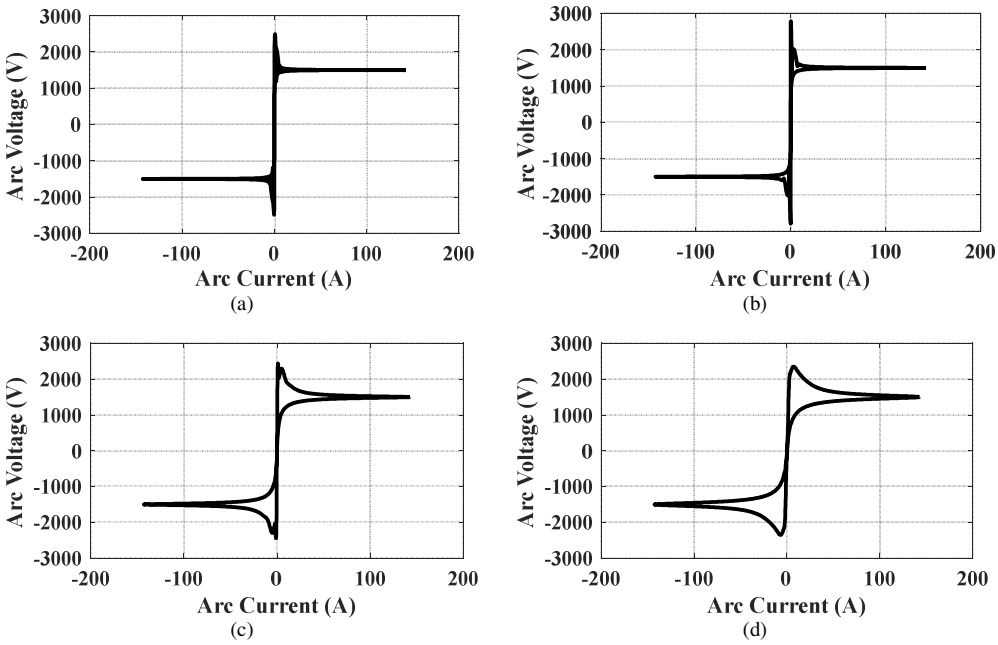

Fig. 1. V–I characteristics at U_{st} equal to 1500 V and τ equal to: (a) 6 µs, (b) 10 µs, (c) 50 µs, and (d) 100 µs.

The effect of the arc time constant on current and voltage waveforms is illustrated in Figures 2 and 3. Both evaluated at a U_{st} of 1500 V. The top subplot (blue line) of each figure presents the arc current, which follows a sinusoidal pattern and reaches zero at approximately 0.22 s, marking the point of current interruption. The lower subplot (red line) depicts the corresponding arc voltage, where the influence of the τ becomes evident.

In Figure 2, corresponding to τ equal to 6 µs, the arc voltage waveform exhibits a nearly square shape with abrupt transitions between positive and negative peaks. This behavior reflects the arc's limited thermal inertia, allowing the voltage to follow the current instantaneously. Therefore, when the current crosses zero, the arc is rapidly extinguished, indicating low stability.

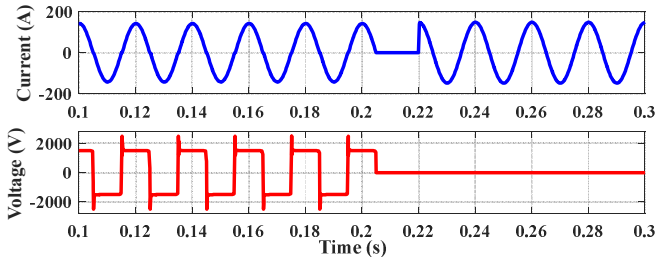

Fig. 2. Current and voltage waveforms at τ equal to 6 µs.

In contrast, Figure 3 obtained at a τ value of 100 µs, revealing a voltage waveform with rounded, gradual transitions rather than sharp edges. This response is attributed to the higher thermal inertia of the arc, which prevents instantaneous voltage changes. As the current reaches zero, the arc voltage rises non-linearly to restrike, thus sustaining the discharge.

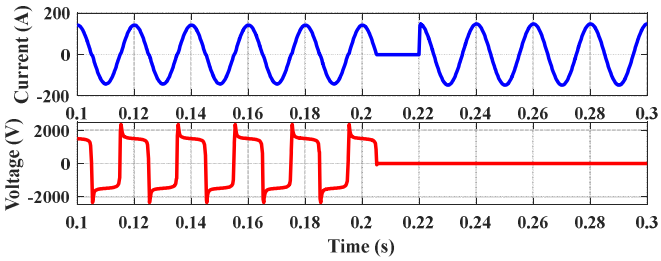

Fig. 3. Current and voltage waveforms at τ equal 100 µs.

The influence of the U_{st} on the V–I characteristics of an electric arc is depicted in Figure 4. The curves reveal that increasing U_{st} significantly modifies the hysteresis loop. A higher U_{st} results in both a wider and taller loop, indicating that the arc can persist over a larger current range and requires a greater restriking voltage once the current passes through zero. This behavior demonstrates that U_{st} plays a decisive role in arc stability, as elevated voltages supply additional energy to sustain the discharge, thereby making extinction more difficult. Consequently, the U_{st} emerges as a critical parameter in evaluating the performance of arc interruption systems.

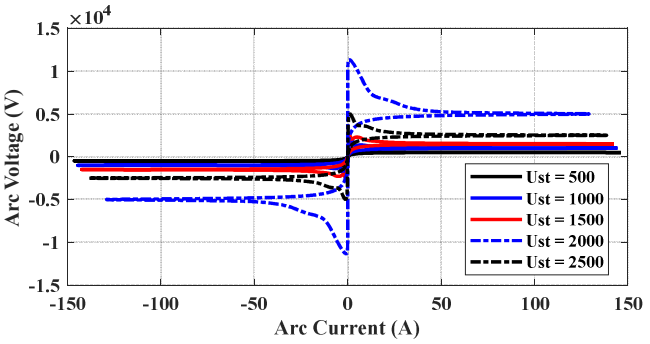

Fig. 4. Effect of U_{st} on the V–I arc characteristics.

Furthermore, Figure 5 highlights how the U_{st} influences the current and voltage waveforms of an electric arc when the time constant is fixed at a τ value of 100 µs. The current largely retains its sinusoidal form, although its amplitude decreases as U_{st} rises. This can be attributed to the nonlinear dependence of arc resistance on voltage: higher values of U_{st} correspond to a greater effective resistance, which in turn restricts current flow. The voltage waveform, however, is more strongly affected. Larger U_{st} values lead to noticeably higher arc voltage amplitudes, as seen when comparing U_{st} of 2500 V and 1500 V against 500 V. At the same time, arcs with higher U_{st} exhibit more pronounced restriking spikes at the current zero, reflecting their higher thermal inertia and greater stability.

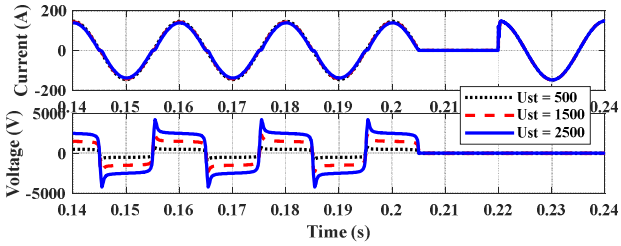

Fig. 5. Current and voltage waveforms at τ equal to 100 µs.

IV. PROPOSED CHIRP SIGNAL ANALYSIS FOR UNIVERSAL ARC DETECTION

To reliably capture the arc signatures in pantograph–catenary systems, time–frequency domain techniques, such as the HHT and the DWT, are widely employed. These methods are particularly suited for arc detection, associating highly non-linear and non-stationary signals, exhibiting time-varying frequency content influenced by the aforementioned system parameters [3, 9, 10].

In the HHT, the signal is first decomposed via Empirical Mode Decomposition (EMD) into a set of Intrinsic Mode Functions (IMFs), each providing a well-defined instantaneous frequency representation. When the Hilbert transform is applied to the IMFs, it gives the time-varying frequency and amplitude, and the instantaneous amplitude of a selected mode can be used as a feature and compared with a threshold to detect arcs. This makes it possible to track chirp-like transients with good accuracy and high time–frequency resolution. In comparison, the DWT breaks the signal into time-based frequency components by scaling and shifting a mother wavelet. Although being effective for transient detection, its accuracy depends heavily on the chosen wavelength and decomposition level. Accordingly, the Hilbert transform is more reliable, especially for chirp-like patterns, and is more effective for pantograph arc detection [3].

From the comparison between the DWT and the HHT, the proposed model uses the Hilbert transform due to its ability to capture chirp-like and transient arc patterns more effectively. The detection algorithm is organized into five main steps, which are illustrated in Figure 6.

The Hilbert transform $Y(t)$ of a signal $X(t)$ is mathematically defined by [3]:

$$Y(t) = H\{X(t)\} = \frac{1}{\pi} P \int_{-\infty}^{\infty} \frac{X(\tau)}{t-\tau} d\tau \quad (3)$$

where P denotes the Cauchy principal value. In this context, $X(t)$ and $Y(t)$ represent the real and imaginary components, respectively, of the corresponding analytic signal Z(t), which can be calculated by:

$$Z(t) = X(t) + j\,Y(t) \quad (4)$$

The instantaneous amplitude (envelope) is defined by:

$$e(t) = |Z(t)| = \sqrt{X^2(t) + Y^2(t)} \quad (5)$$

In this algorithm, $X(t)$ represents the time derivative of the filtered current signal, so e(t) captures the instantaneous magnitude of derivative fluctuations caused by arcing.

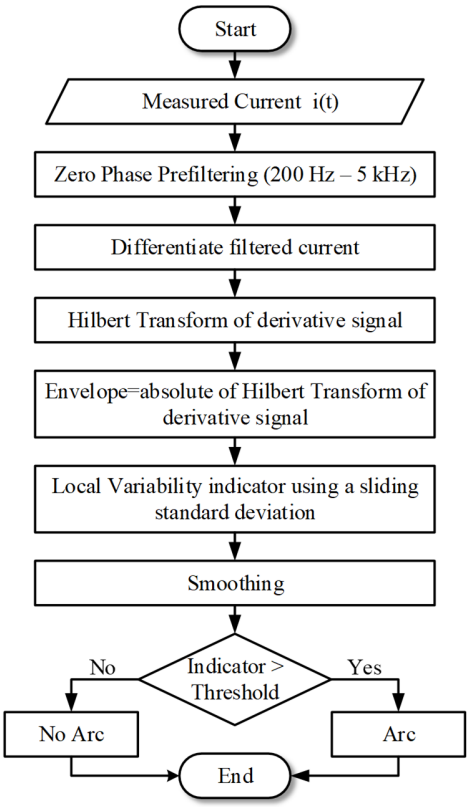

Fig. 6. Flowchart of the proposed arc detection algorithm for pantograph–catenary systems.

Moreover, a sliding standard deviation is computed over a centered moving window of a duration of approximately 4 ms. This operation emphasizes periods of rapid fluctuation in the derivative envelope while suppressing steady-state intervals. A moving standard deviation is computed over a short window Δ_1 by:

$$s(t) = \sqrt{\frac{1}{N_1}\sum_{k=0}^{N_1-1}[e(t-k)-\bar{e}(t)]^2} \quad (6)$$

where N_1 is the number of samples in Δ_1 and $\bar{e}(t)$ is the mean envelope value within the window. Furthermore, the algorithm smooths this variability measure by computing a sliding absolute sum over a longer window Δ_2 of approximately 10 ms. This step aggregates fluctuations, making the index more robust against single-sample spikes or noise. The moving absolute sum of $s(t)$ is depicted by:

$$J(t) = \sum_{k=0}^{N_2-1}|s(t-k)| \quad (7)$$

where N_2 is the number of samples in Δ_2. Finally, arc events are detected by comparing J(t) to a fixed threshold, calculated by:

$$d_{arc}(t) = \begin{cases} 1, & if\ J(t) > Threshold \\ 0, & if\ J(t) < Threshold \end{cases} \quad (8)$$

The use of robust statistical measures prevents false triggering from isolated noise peaks. This complete sequence ensures precise arc detection while minimizing false positives and maintaining a stable post-extinction baseline, even under varying environmental and operational conditions.

V. PERFORMANCE EVALUATION OF PROPOSED CHIRP SIGNAL ANALYSIS

The algorithm is evaluated for an arc case with a time constant of a τ value of 6 µs and a U_{st} value of 1500 V. The corresponding transient current, after processing with a zero-phase band-pass filter, is presented in Figure 7. The filtering effectively suppresses low-frequency drift and high-frequency noise, isolating the transient components of the arc current. The resulting waveform exhibits a pronounced spike followed by damped oscillations around 0.22 s. After this point, the current rapidly falls to zero. This distinct transient signature indicates an arc extinction or a significant circuit interruption.

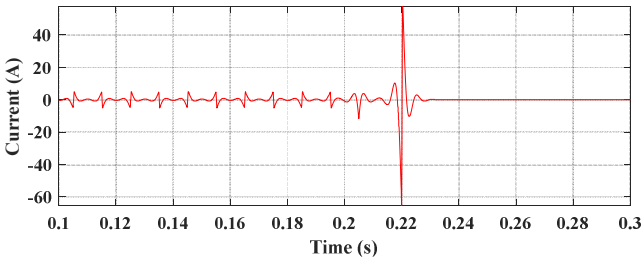

Fig. 7. Filtered arc current waveform at τ equal to 6µs and U_{st} to 1500V.

The imaginary component of the analytic signal, obtained by applying the Hilbert transformation to the differentiated and pre-filtered current, is displayed in Figure 8. Prior to 0.21 s, the waveform presents periodic oscillations caused by load dynamics or pantograph–catenary interaction. At approximately 0.21 s, a sharp high-amplitude excursion appears, representing the transient response associated with arc ignition. Once the event subsides, the signal rapidly returns to near-zero, confirming the absence of strong high-frequency components in the post-arc steady state. It extracts the quadrature component required for constructing the instantaneous envelope in the subsequent analysis.

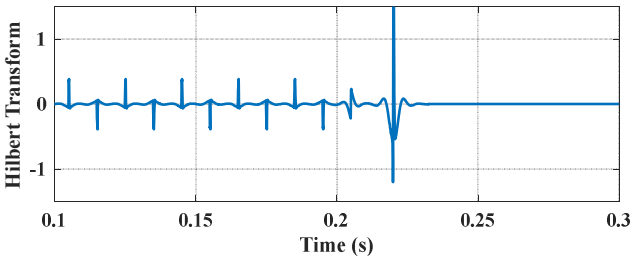

Fig. 8. Hilbert transformation of the pre-filtered current derivative

Figure 9 illustrates the instantaneous amplitude of the current derivative. Periodic peaks appear before 0.21 s, corresponding to mechanical vibrations or commutation noise in the pantograph–catenary interface. The large, isolated peak

at 0.21 s is due to the arc transient, whose magnitude exceeds normal fluctuations. This transformation effectively rectifies the derivative fluctuations and removes sign information, leaving only the instantaneous magnitude of transient activity.

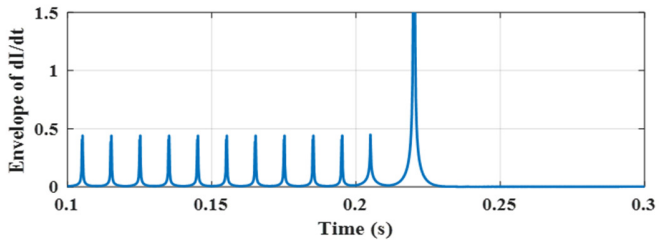

Fig. 9. Instantaneous envelope of the current derivative.

Moreover, Figure 10 portrays the moving standard deviation of the envelope signal $e(t)$ computed over a 4 ms sliding window. This statistical measure emphasizes localized variability rather than absolute amplitude, making it effective for identifying genuinely fluctuating arc-like behavior. In the pre-event region, the standard deviation remains nearly constant, reflecting a stable oscillatory behavior. At 0.21 s, a sharp rise occurs, capturing the heightened volatility during the arc transient. After the arc ends, the standard deviation quickly decays, confirming the event's short duration.

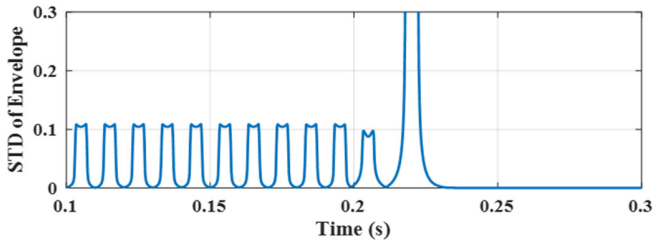

Fig. 10. Sliding standard deviation of the envelope at a 4 ms window.

To validate the robustness of the proposed algorithm, the range of evaluations is increased along with the number of tests at different voltages and τ values, as shown in Table I.

TABLE I. ARC DETECTION TEST CASE MATRIX

U_{st} (V)	Case number			
	6 µs	*10 µs*	*50 µs*	*100 µs*
500	1	3	4	5
1000	7	9	10	11
1500	2	6	8	12
2000	14	18	19	20
2500	13	15	16	17

The absolute sum index, evaluated over a 10 ms sliding window, is presented in Figure 11. The threshold-based binary decision signal is illustrated in Figure 12. The resulting clean, noise-free binary output demonstrates the robustness of the detection approach.

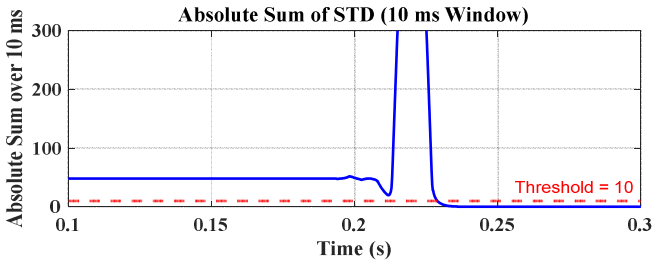

Fig. 11. Absolute sum of envelope standard deviation (blue solid line) and detection threshold (red dashed line).

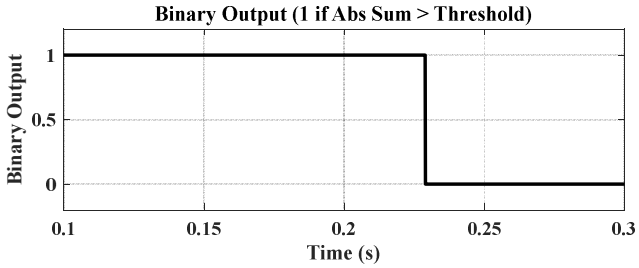

Fig. 12. Binary arc detection output. A value of 1 indicates the presence of arc activity, while a value of 0 indicates its absence.

Furthermore, Figure 13 depicts the Hilbert transform of the pre-filtered current derivative across 20 pantograph–catenary test cases, highlighting transient fluctuations for envelope extraction. The sensitivity of the Hilbert transformation is exhibited by oscillatory patterns with varying amplitudes and frequencies of the traces. The band-pass pre-filtering (200 Hz–5 kHz) ensures that only relevant transients are enhanced, minimizing noise artifacts in $Y(t)$.

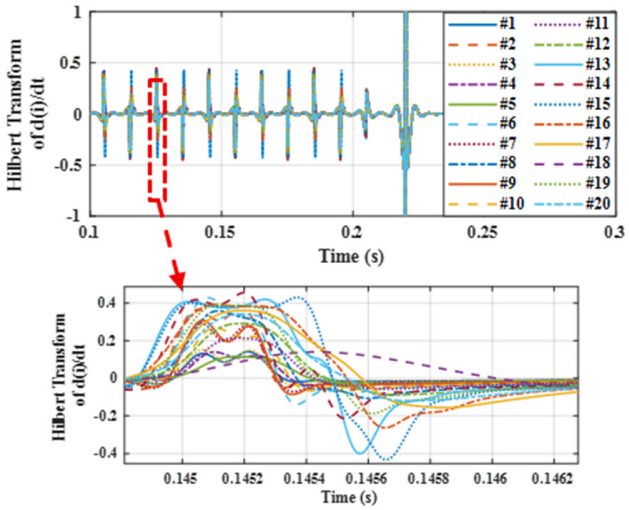

Fig. 13. Enlarged view of the Hilbert transform at different test cases.

Figure 14 highlights the algorithm's final stage before thresholding. The use of median absolute deviation in threshold selection ensures minimal false positives, even in noisy environments. Comparatively, cases with correlated high oscillations tend to produce elevated $J(t)$ values, demonstrating

the algorithm's coherent progression from raw transients to a reliable detection index.

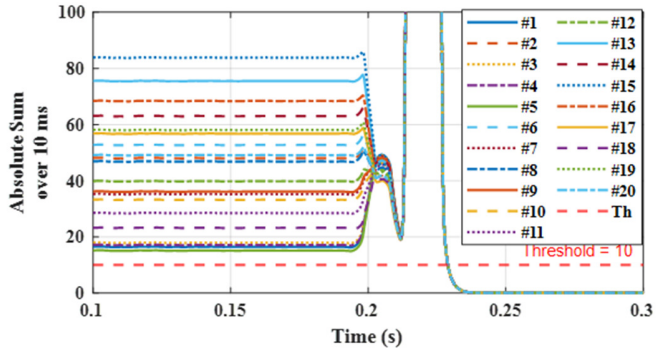

Fig. 14. Time-varying sliding absolute sum of the envelope.

Table II presents the index of the absolute sum of the envelope standard deviation as a function of the U_{st} and the τ. The U_{st} values range from 500 V to 2500 V, while τ varies between 6 µs to 100 µs. The results indicate that the index increases with higher values for all tested τ, reflecting a stronger arc-induced fluctuation. Conversely, for a given U_{st}, the index decreases as τ becomes larger, particularly beyond 50 µs. This behavior demonstrates the sensitivity of the proposed metric to both the U_{st} and the dynamic arc response characterized by τ. Specifically, the lowest value of the index is 15.15 at U_{st} equal to 500 V and τ equal to 100 µs, while the maximum value reached 83.9 at U_{st} equal to 2500 V and τ equal to 10 µs. Based on these results, the threshold is chosen to be 10, ensuring that it remains lower than the minimum observed index value.

TABLE II. ABSOLUTE SUM OF ENVELOPE STANDARD DEVIATION INDEX

U_{st} (V)	Deviation index			
	6 µs	*10 µs*	*50 µs*	*100 µs*
500	16.5	17.9	17.12	15.15
1000	35.15	36.11	33.24	28.51
1500	48.01	52.69	46.8	39.8
2000	63.1	66.39	57.9	49.11
2500	75.5	83.9	68.5	56.7

The results from Figures 13, 14, and Table II demonstrate the performance of the Hilbert transformation and the corresponding sliding absolute sum of the envelope across a wide range of arc parameters, confirming the validity of the proposed detection method. The method remained effective even during the arc plasma's varied behavior. This adaptability allowed the algorithm to track arc dynamics under different conditions and to provide consistent arc detection across a wide range of operating scenarios.

VI. CONCLUSIONS

This paper introduced a chirp-based detector for pantograph arc identification as an alternative to image-driven techniques. The approach relies on current signal processing, combining band-pass filtering between 200 Hz and 5 kHz, differentiation, and Hilbert transformation analysis, followed by statistical evaluation. A sliding standard deviation window of 4 ms, along with a 10 ms absolute sum window, was employed to highlight the arc activity while reducing the influence of noise and single-sample fluctuations. In addition, the use of median absolute deviation minimizes false triggering. The proposed algorithm was tested under 20 different cases that covered a wide range of stationary voltage (U_{st}) and arc time constant (τ) values. The evaluation revealed that the method can reliably detect arc events under all scenarios without the need for image-based processing. The detection index was affected by both U_{st} and τ. As the voltage increased, it became larger and smaller for a longer τ, especially for values above 50 µs. During the test cases, the index ranged from 15.15 at U_{st} = 500 V and τ = 100 µs to 83.9 at U_{st} = 2500 V and τ = 10 µs, highlighting the high sensitivity to arc dynamics. From these values, a threshold of 10 was chosen to ensure reliable detection under all conditions. These findings confirm both the practicality of the approach and its ability to operate effectively in diverse operating conditions.

REFERENCES

[1] G. Gao, T. Zhang, W. Wei, Y. Hu, G. Wu, and N. Zhou, "A pantograph arcing model for electrified railways with different speeds," *Proceedings of the Institution of Mechanical Engineers, Part F: Journal of Rail and Rapid Transit*, vol. 232, no. 6, pp. 1731–1740, Dec. 2017, https://doi.org/10.1177/0954409717747775.

[2] Y. Yan, H. Liu, L. Gan, and R. Zhu, "A novel arc detection and identification method in pantograph-catenary system based on deep learning," *Scientific Reports*, vol. 15, no. 1, Jan. 2025, Art. no. 3511, https://doi.org/10.1038/s41598-025-88109-x.

[3] S. Barmada and M. Tucci, "Use of Advanced Signal Processing Techniques for Arcing Detection on AC Pantograph Catenary Systems," in *Proceedings of International Conference on Pantograph-Catenary Interaction Framework for Intelligent Control*, Amiens, France, Dec. 2011, pp. 1–7.

[4] Y. Liu *et al.*, "A Novel Arcing Detection Model of Pantograph–Catenary for High-Speed Train in Complex Scenes," *IEEE*, vol. 72, pp. 1–13, Apr. 2023, https://doi.org/10.1109/TIM.2023.3267365.

[5] S. Huang, Y. Zhai, M. Zhang, and X. Hou, "Arc detection and recognition in pantograph–catenary system based on convolutional neural network," *Information Sciences*, vol. 501, pp. 363–376, June 2019, https://doi.org/10.1016/j.ins.2019.06.006.

[6] R. Chen, Y. Lin, and T. Jin, "High-Speed Railway Pantograph-Catenary Anomaly Detection Method Based on Depth Vision Neural Network," *IEEE Transactions on Instrumentation and Measurement*, vol. 71, pp. 1–10, July 2022, https://doi.org/10.1109/TIM.2022.3188042.

[7] Y. Luo, Q. Yang, and S. Liu, "Novel Vision-Based Abnormal Behavior Localization of Pantograph-Catenary for High-Speed Trains," *IEEE Access*, vol. 7, pp. 180935–180946, Nov. 2019, https://doi.org/10.1109/ACCESS.2019.2955707.

[8] H. A. Darwish, M. Hesham, A.-M. I. Taalab, and N. M. Mansour, "Close Accord on DWT Performance and Real-Time Implementation for Protection Applications," *IEEE Transactions on Power Delivery*, vol. 25, no. 4, pp. 2174–2183, Aug. 2010, https://doi.org/10.1109/TPWRD.2009.2036401.

[9] W. Liu, X. Zhang, Y. Dong, and X. Huang, "Arc fault detection for AC SSPC based on Hilbert-Huang transform," in *Proceedings of 43rd Annual Conference of the IEEE Industrial Electronics Society*, Beijing, China, Oct. 2017, pp. 4104–4109, https://doi.org/10.1109/IECON.2017.8216704.

[10] Darwish, Farouk, Taalab, and Mansour, "Investigation of Real-Time Implementation of DSP-Based DWT for Power System Protection," in *Proceedings of IEEE/PES Transmission and Distribution Conference and Exhibition*, Dallas, TX, USA, May 2006, pp. 1258–1263, https://doi.org/10.1109/TDC.2006.1668691.

[11] B. Sundararaman and P. Jain, "Fault Detection and Classification in Electrical Power Transmission System Using Wavelet Transform," *Engineering Proceedings*, vol. 59, no. 1, Dec. 2023, , Art. no. 71, https://doi.org/10.3390/engproc2023059071.

[12] N. I. Elkalashy, M. Lehtonen, H. A. Darwish, A.-M. I. Taalab, and M. A. Izzularab, "DWT-Based Detection and Transient Power Direction-Based Location of High-Impedance Faults Due to Leaning Trees in Unearthed MV Networks," *IEEE Transactions on Power Delivery*, vol. 23, no. 1, pp. 94–101, Jan. 2008, https://doi.org/10.1109/TPWRD.2007.911168.

[13] D. Uhrlandt *et al.*, "Electrical models of arcs in different applications," *PLASMA PHYSICS AND TECHNOLOGY*, vol. 11, no. 1, pp. 28–35, May 2024, https://doi.org/10.14311/ppt.2024.1.28.

[14] Z. Wang, Z. Li, C. Han, and F. Guo, "Mathematical Model of Pantograph Arc Based on Probability Distribution of Arc Parameters," *IEEE Transactions on Transportation Electrification*, vol. 9, no. 2, pp. 2026–2037, Oct. 2023, https://doi.org/10.1109/TTE.2022.3217049.

[15] Y.-J. Liu, G. W. Chang, and H. M. Huang, "Mayr's Equation-Based Model for Pantograph Arc of High-Speed Railway Traction System," *IEEE Transactions on Power Delivery*, vol. 25, no. 3, pp. 2025–2027, June 2010, https://doi.org/10.1109/TPWRD.2009.2037521.

[16] Y. Wang, Z. Liu, X. Mu, K. Huang, H. Wang, and S. Gao, "An Extended Habedank's Equation-Based EMTP Model of Pantograph Arcing Considering Pantograph-Catenary Interactions and Train Speeds," *IEEE Transactions on Power Delivery*, vol. 31, no. 3, pp. 1186–1194, Nov. 2016, https://doi.org/10.1109/TPWRD.2015.2500260.

[17] Z. Xu *et al.*, "Characteristics of pantograph-catenary arc under low air pressure and strong airflow," *High Voltage*, vol. 7, no. 2, pp. 369–381, Dec. 2022, https://doi.org/10.1049/hve2.12180.

[18] N. V. Hai, N. V. Tiem, L. H. Lan, and T. H. Vo, "Pantograph Catenary Contact Force Regulation Based on Modified Takagi-Sugeno Fuzzy Models," *Engineering, Technology & Applied Science Research*, vol. 13, no. 1, pp. 9879–9887, Feb. 2023, https://doi.org/10.48084/etasr.5443.

[19] A. Iturregi, B. Barbu, E. Torres, F. Berger, and I. Zamora, "Electric Arc in Low-Voltage Circuit Breakers: Experiments and Simulation," *IEEE Transactions on Plasma Science*, vol. 45, no. 1, pp. 113–120, Dec. 2016, https://doi.org/10.1109/TPS.2016.2633400.

[20] H.-J. Odenthal, A. Kemminger, F. Krause, L. Sankowski, N. Uebber, and N. Vogl, "Review on Modeling and Simulation of the Electric Arc Furnace (EAF)," *steel research international*, vol. 89, no. 1, Nov. 2017, Art. no. 1700098, https://doi.org/10.1002/srin.201700098.